Surface Science 69 (1977) 62–84

SURFACE ELECTRONIC AND CHEMICAL STRUCTURE OF (11$\bar{2}$0)CdSe: COMPARISON WITH CdS

L.J. BRILLSON
Xerox Webster Research Center, Webster, New York 14580, USA

Received 14 June 1977; manuscript received in final form 12 July 1977

Surface photovoltage spectroscopy, Auger electron spectroscopy, LEED, X-ray and ultraviolet photoemission measurements are reported for (11$\bar{2}$0) CdSe under a variety of ultrahigh vacuum conditions. As with CdS, all surface electronic features can be related to chemical contamination, Ar^+ bombardment-induced lattice defects, or bulk trap states. Oxygen adsorption on CdSe and CdS produce qualitatively different electronic features which are attributed to different bonding at surface vacancy sites. Changes in surface atomic order show no direct effect on measured electronic features. Furthermore, CdSe exhibits no intrinsic surface state features which can account for its Schottky barrier formation with metals.

1. Introduction

CdSe and CdS possess chemical bonding and bulk electronic properties which lie midway between those of covalent and ionic semiconductors. These representative semiconductors also span a transition between covalent and ionic materials in their characteristics of interface barrier formation with metals [1]. The insensitivity of Schottky barrier height to various metals on CdSe relative to the same metal-CdS interfaces has been attributed to Fermi level stabilization at surface states of the more covalent CdSe [2,3]. In turn, such states could arise from distortion of the lattice potential at the surface [4,5], which is more severely disturbed for covalent than ionic solids. CdSe and CdS are also widely used photoconductors whose transport properties, particularly for thin films, are strongly affected by different surface treatments [6]. Since these homologous compound semiconductors differ primarily in their binding, comparison of their surface electronic structures reveals the effect of bonding changes as well as their influence on surface and interface electrical properties.

The surface electronic structure of (11$\bar{2}$0) CdSe was determined by surface photovoltage spectroscopy (SPS) for a variety of surface conditions whose chemical structure was measured by Auger electron spectroscopy (AES), LEED, and X-ray photoelectron spectroscopy (XPS). This work complements a similar study on CdS reported earlier [7]. We find that all surface electronic features detected by SPS can

be correlated with extrinsic surface states produced by chemical contamination (e.g. air exposure, oxidation) or by lattice nonstoichiometry produced by Ar^+ bombardment. SPS also revealed a bulk trap level in the band gap of all CdSe crystals studied. Changes in surface atomic order had no measurable effect on surface electronic features. A mechanism of oxygen adsorption involving lattice vacancies at CdSe and CdS surfaces is proposed to account for the qualitative difference in their adsorbate electronic features. The results presented here also show that CdSe and CdS possess no difference in intrinsic surface state structure which can account for their dissimilarity in Schottky barrier formation with metals. This conclusion underscores the importance of extrinsic surface phenomena in determining the interfacial electrical phenomena of these materials.

A description of the UHV techniques used to characterize the surface electronic and chemical structure of CdSe is given in section 2. The results of SPS, AES, LEED, XPS, and ultraviolet photoelectron spectroscopy (UPS) measurements on $(11\bar{2}0)$ CdSe are presented in section 3. Both filled and empty surface states within the band gap are determined by SPS and related to chemical structure monitored by AES, XPS, and LEED for the same surfaces. Surface and bulk photoconductivity spectra are also presented for the determination of bulk trap states. Section 4 includes a discussion of these spectra with respect to the electronic and chemical features of CdS and deals with the implication of these results for interface electrical phenomena.

2. Experimental

CdSe surfaces were prepared and analyzed chemically and electronically in a stainless steel chamber with a base prssure $\sim 5 \times 10^{-11}$ Torr (6.5×10^{-9} Pa). This is represented schematically in fig. 1. SPS features were obtained by a vibrating Kelvin reed technique, which was used to monitor surface work function as a function of incident photon energy from a wide-band, Leiss double-prism monochromator ($0.5 < h\nu \lesssim 6$ eV). A detection circuit employing negative feedback from a lock-in amplifier permitted continuous measurements to be made with a stability of $\sim$1 mV. Typically several spectra were summed and smoothed before determining energies of SPS features. Monochromator resolution was ≤ 50 meV, but gradual spectral slope changes limited precision of energy level positions to $\sim$0.1 eV. Additional details of this technique have been described previously [7,8]. The vibrating reference probe was a 1 mmAu boss. Because of its small size, effects of surface inhomogeneity (i.e. roughness) could be studied. In particular, visually smooth surfaces obtained by cleavage could be selected and studied even when the overall cleaved surface displayed some roughness. This is a significant advantage in view of the electronic effects which can be associated with surface roughness [9].

AES and XPS were performed using a double-pass cylindrical mirror analyzer (CMA). The current of the glancing incidence electron gun was kept below 5 μA/

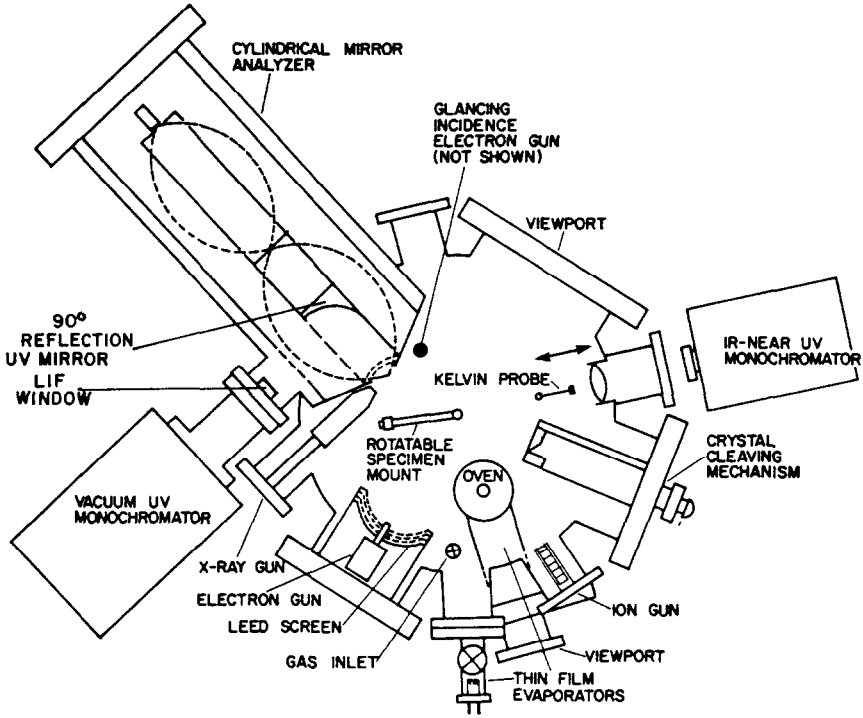

Fig. 1. Schematic top view of the ultrahigh vacuum chamber (base pressure $<5 \times 10^{-11}$ Torr).

mm^2 to minimize electron beam damage. The X-ray source was a 400 W Mg K_α-gun directed at right angles to the CMA axis. Retarding grids at the CMA entrance aperture maintained a constant 1.2 eV resolution for core level spectra and 1 eV for valence band spectra. The CMA was also employed for UPS measurements. As shown in fig. 1, light from a hydrogen discharge lamp passes through a vacuum UV monochromator (McPherson 218) and LiF window into the UHV chamber. An elliptical mirror in the CMA at the intersection of the monochromator and CMA axes focuses the light at the focal point of the electron monochromator. The elliptical mirror segment consists of a machined and polished everdur copper base (compatible with a 300°C bakeout) which was overcoated with Al and MgF_2 [10]. Overall energy resolution was 0.3 eV. Low energy electron loss spectroscopy (ELS) was also performed with this CMA and with the glancing incidence electron gun operated at a primary beam voltage of 100–500 eV. A 1 V p-p modulation voltage limited the energy resolution to 1.2 eV although energy differences could be determined to $\leq$ 0.5 eV. Infrared absorption associated with bulk trap states over the range 2.5 to 0.6 μm was measured with a Cary 17 spectrophotometer. Bulk inhomogeneity within crystals were monitored with an infrared transmission microscope. Surface and bulk photoconductivity measurements were performed in air

using a modified bridge circuit with detectability $\Delta R/R < 10^{-4}$.

The CdSe crystals were 4 X 4 X 15 mm bars oriented with (11$\bar{2}$0) square faces. The (11$\bar{2}$0) face was chosen because it cleaves well and resists facetting at high temperatures [11]. "Ultrahigh-purity" crystals were obtained from both Eagle-Picher Industries and Cleveland Crystals. All crystals were prepared by vapor deposition and had resistivities of ~1 ohm-cm in order to minimize any Dember voltage [12] or any charging during AES, XPS, UPS, ELS or LEED measurements. The surfaces were polished with 1.0 μm Al_3O_3 followed by "Lustrox 1000", and then etched in H_3PO_4 at 185°C. Ohmic contacts were prepared by Ar^+ bombardment cleaning in UHV followed by Al evaporation [13]. These contacts can withstand high temperature annealing, whereas conventional ohmic contacts consisting of In do not. Clean crystal surfaces could be prepared by Ar^+ bombardment or cleavage in UHV. High temperature annealing, oxidation, and thin film evaporation could also be performed in situ.

3. Results

The surface chemical composition of (11$\bar{2}$0) CdSe was monitored by AES and XPS, while the surface electronic structure was determined by SPS. Results of these measurements are composed for air-exposed, UHV-cleaved, Ar^+ bombarded, annealed, and oxygen-adsorbed surfaces.

3.1. Chemical structure of (11$\bar{2}$0) CdSe

The chemical compositions of (11$\bar{2}$0) CdSe surfaces prepared under a variety of conditions were studied by AES. Representative spectra are illustrated in fig. 2. Curve a indicates that a polished and etched surface is considerably contaminated with S, Cl, C. and O, even after prolonged UHV exposure under illumination. The Auger electron spectrum of this surface after a 150°C bakeout is shown in fig. 2b. The spectrum shows similar contamination with proportionally more C, indicating that mild heating is insufficient to remove contamination from an air-exposed surface.

A "clean" stoichiometric (11$\bar{2}$0) surface was obtained by UHV cleavage. Only the characteristic Se and Cd Auger structures were detected as shown in fig. 2c. With a 50 μA incident ion current, a detectability limit for any contamination present was estimated to be <1% monolayer equivalent. No contamination was detected on this surface even after several days exposure at 10^{-10} Torr.

Since the cleaved (11$\bar{2}$0) surface is stoichiometric, the peak-to-peak Auger intensity ratio Se (1315 eV)/(Cd (276 eV) of this surface could be used to calibrate relative nonstoichiometries of other surfaces. For example, fig. 2d indicates that 1 keV Ar^+ bombardment for 20 min at 50 μA produces a relative increase in the Se (1315 eV)/Cd (376 eV) ratio of as much as 20%. This can be associated with Se

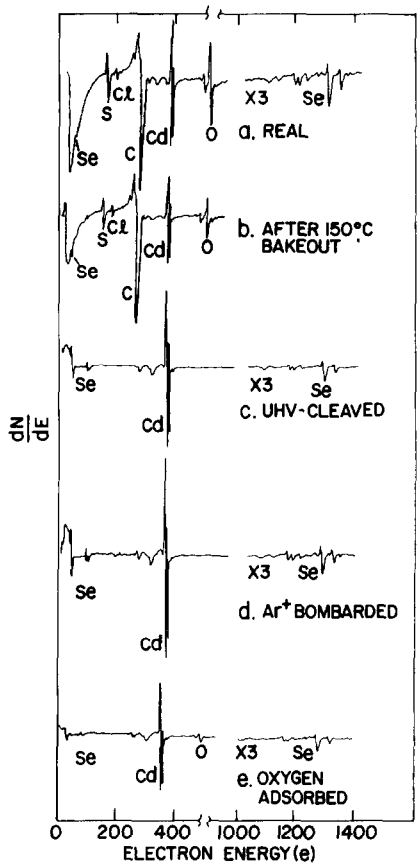

Fig. 2. Auger electron spectra of (11$\bar{2}$0) CdSe under various surface conditions: (a) polished and etched in air and after 24 h at $p = 10^{-9}$ Torr; (b) same surface after 6 h, 150°C bakeout; (c) UHV-cleaved; (d) Ar^+ bombarded; (e) oxygen-adsorbed. All spectra were obtained with primary energy $E_p = 3$ keV except (b) (2 keV), primary beam current $I_p \leq 5.0$ μA, and peak-to-peak modulation voltage $V_m = 2$ eV.

diffusion to the surface, analogous to S in CdS [7,14]. The surface nonstoichiometry measured by AES can be almost completely eliminated by annealing. After a 4 h anneal at 400°C, the surface also exhibited a LEED pattern typical of clean, ordered (11$\bar{2}$0) CdSe. The cleaved (11$\bar{2}$0) face shows only a faint LEED pattern due to surface charging. This charging is reduced after Ar^+ bombardment and annealing because of the lower resistivity associated with the Se vacancies left below the surface layer. Similar effects are observed for CdS [7]. Continued annealing further improved the sharpness of (11$\bar{2}$0) CdSe LEED patterns. However, annealing at 400°C is known to cause sublimation of Se and S from the CdSe and CdS surface respectively [15]. Diffusion of Cd to the surface has also been reported

for CdSe annealed at $T \geq 400°C$ [16]. The contrasting LEED quality of cleaved versus Ar^+ bombarded and annealed surfaces suggests that the latter may not be typical of the stoichiometric, unreconstructed lattice [17,18].

Two methods were used to adsorb oxygen on (11$\bar{2}$0) CdSe. First, the UHV chamber was backfilled from 10^{-10} Torr with high purity oxygen to atmospheric pressure and the "clean" CdSe surface characterized by AES or XPS was exposed for various time intervals. The resultant coverages measured at $p < 10^{-8}$ Torr from XPS spectra yielded sticking coefficients $S \sim 10^{-13}$. These extremely small values are consistent with the low sticking coefficients observed for clean, ordered CdS by surface conductivity [19]. Exposure of CdSe to oxygen positioned ~1 inch from a hot (1700°C) W filament at $p = 10^{-5}$ Torr (1.3×10^{-3} Pa) [17] resulted in much higher sticking coefficients $S \sim 2 \times 10^{-4}$. Similar activated oxygen adsorption has been reported recently for III–V compounds [20]. This hot filament (HF) technique was particularly desirable because the equivalent monolayer surface coverage θ could be varied by small increments and could be increased to full surface coverage ($\theta = 1.0$), in contrast to the high pressure (HP) technique. On the other hand, some W contamination ($\theta < 0.1$) was also found to be associated with this method, possibly as a WO_3 adsorbate. Nevertheless both techniques yielded similar SPS spectra, as will be shown. UV illumination from a Xe lamp promoted no measurable increase in oxygen adsorption rates for either technique, although it did produce transient charges in surface photovoltage which were consistent with previous observations [21].

Surface chemical characterization of oxygen-exposed surface was carried out primarily using XPS, since the AES electron beam slowly desorbed the oxygen adsorbate. For example, the O (510 eV)/Cd (376 eV) Auger peak intensity ratio of a partially oxidized (11$\bar{2}$0) CdSe surface decreased by more than 40% after a 15 min exposure to a 10 $\mu A/mm^2$ incident electron beam. On the other hand, no oxygen desorption was detectable during the course of XPS measurements. XPS intensities were normalized using a recent calibration of relative X-ray photoionization cross sections [22]. Assuming that oxygen adsorbs in a uniform overlayer, absolute oxygen surface coverages were determined from ratios of the O $1S_{1/2}$ (532 eV) and Cd $3d_{5/2}$ (404 eV) peak heights normalized by their respective photoionization cross sections. A representative XPS spectrum of oxygen-adsorbed (11$\bar{2}$0) CdSe is shown in fig. 3. The coverages were corrected for attenuation by the oxygen overlayer, using a mean free path $D = 9$ Å [23] and an overlayer thickness $d \sim 4.5$ Å based on the CdO lattice spacing $a_0 = 4.7$ Å [24]. The peak height ratio $I(O\ 1s_{1/2})/I(Cd\ 3d_{5/2})$ was observed to saturate at a corresponding surface coverage $\theta = 0.98$. The coverage versus exposure curve is illustrated in fig. 4. The initial slope corresponds to a sticking coefficient $S = 2.2 \times 10^{-4}$. The absence of any discontinuity in the monotonic curve indicates that no special site or multi-particle adsorption processes take place at intermediate coverages. Oxygen adsorption on the initially LEED-ordered (11$\bar{2}$0) surface produced no new diffraction beams, suggesting either random site adsorption or very short range ordering. At a surface coverage θ

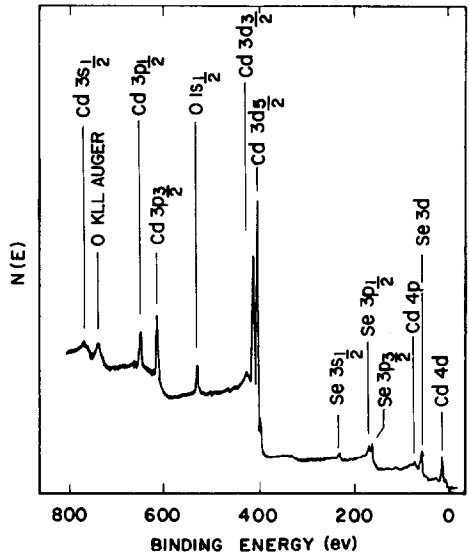

Fig. 3. Representative XPS spectrum of oxygen adsorbed (11$\bar{2}$0) CdSe used in determining oxygen surface coverage. Binding energies are given with respect to the Mg K_α source energy of 1253.6 eV.

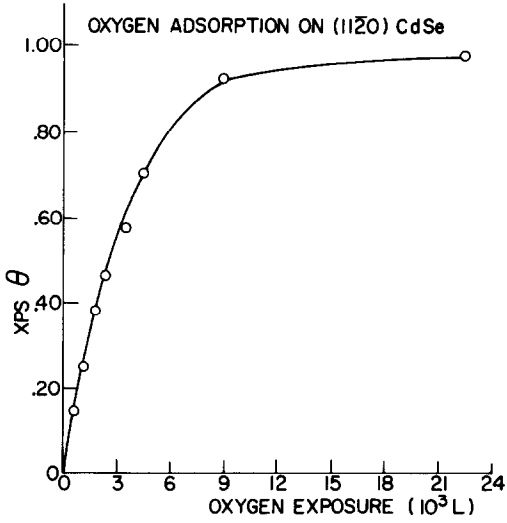

Fig. 4. Surface coverage of oxygen on LEED-ordered, (11$\bar{2}$0) CdSe as a function of exposure (1 L = 10^{-6} Torr sec) in the presence of a 1700° W filament.

= 0.1, the LEED pattern was noticeably less distinct and at monolayer coverages, it disappeared altogether. These effects were also observed for oxygen adsorption on a (11$\bar{2}$0) surface at 100 K. The saturation coverage shown in fig. 3 agree with the saturation exposure of 2.4×10^3 Langmuir for oxygen on CdS reported by Farnsworth based on changes in LEED intensity [17]. Thus the limiting surface coverage for oxygen on (11$\bar{2}$0) CdSe is one monolayer.

Oxidation also produces a relative decrease in Se to Cd surface atoms as measured by the Se (44 eV)/Cd (376 eV) Auger peak height ratios in figs. 2c and 2e. The Se (1315 eV)/Cd (376 eV) Auger peak height ratio also decreases with oxidation, but by a smaller amount, consistent with the larger escape depth of Se (1315 eV) versus Se(44 eV) Auger electrons from the bulk. Similarly, a decrease of the intensity ratio $I(\mathrm{Se}\ 3p_{3/2})/I(\mathrm{Cd}\ 3d_{5/2})$ with oxidation is observed by XPS, This phenomenon can be accounted for by a preferential "shadowing" of Se atoms as oxygen bonds to surface Cd sites. Ref. [7] includes a description of analogous "shadowing" of S atoms by oxygen on (11$\bar{2}$0) CdS. This preferential adsorption and the gradual LEED changes are compatible with a random distribution of microscopic oxygen patches with very short-range ordering. A comparable decrease in the $I(\mathrm{Se}\ 3p_{3/2})/I(\mathrm{Cd}\ 3d_{5/2})$ XPS peak height ratio was also observed for oxygen adsorption by the HP technique. However, the highest surface coverage obtained by this method was $\theta_{\mathrm{XPS}} = 0.4$ In either case, adsorption is not controlled by charge transfer through the surface space charge region, which would limit surface coverage to $S \lesssim 10^{-3}$ [11,12]. Finally, oxygen adsorbed by either technique showed no measurable desorption after several hours in the illuminated chamber, indicating that surface conditions did not change significantly during the SPS measurements of oxygen adsorbed on CdSe.

3.2. Electronic structure of (11$\bar{2}$0) CdSe

Surface electronic structure within the bandgap of CdSe was measured primarily by SPS. XPS and, to some extent, UPS were used to investigate changes in valence band structure. ELS measurements have previously been used to monitor changes in surface electronic structure above the valence band edge due to oxidation [25].

Fig. 5 illustrates SPS spectra for (1120) CdSe under a variety of surface conditions corresponding to the Auger spectra of fig. 2. The contact potential difference (cpd) between the Au reference probe and the (11$\bar{2}$0) CdSe surface was measured as a function of incident photon energy $h\nu$. Changes in cpd slope with energy correspond to onsets of transitions which either populate or depopulate energy levels within the bandgap. A positive $\Delta\mathrm{cpd}/\Delta h\nu$ slope change at an energy $E_0 = h\nu_0$ corresponds to a transition which empties charge from a level E_0 below the conduction band edge. Conversely, a negative $\Delta\mathrm{cpd}/\Delta h\nu$ slope change at an energy E_1 corresponds to a transition filling a level E_1 above the valence band. A more complete description of SPS is given elsewhere [8].

The changes in SPS features of fig. 5 with different surface conditions show that

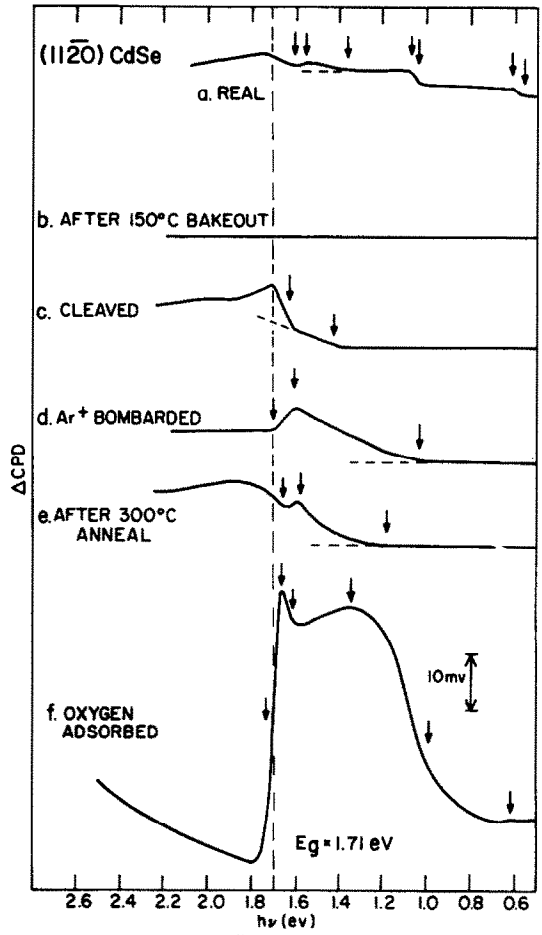

Fig. 5. Surface photovoltage spectra of (11$\bar{2}$0) CdS under various surface conditions: (a) polished and etched in air and after 24 h at 10^{-9} Torr; (b) same surface after 150°C bakeout; (c) UHV-cleaved (d) Ar^+ bombarded; (e) Ar^+ bombarded and annealed for 5 h at 300°C; (f) oxygen-adsorbed with 3×10^{12} L O_2 exposure.

these features are due to changes in surface electronic structure and not due to bulk effects. The increase in $\Delta cpd/\Delta h\nu$ occurring just below the 1.71 eV band gap energy [26] for several of these spectra corresponds to band-to-band transitions which cause a reduction in band bending within the surface space charge region. The polished, etched, and air-exposed CdSe surface exhibits SPS features shown in fig. 5a corresponding to C, O, S. and Cl contamination. The negative $\Delta cpd/\Delta h\nu$ slope changes are due to transitions from levels 1.55, 1.07, and 0.6 eV below the conduction band edge. The positive $\Delta cpd/\Delta h\nu$ slope changes correspond to transitions to levels 1.36, 1.04, and 0.56 eV above the valence band edge. The comple-

mentary transitions 1.07 and 0.56 eV and 1.04 and 0.61 eV are both seen to add up to the absorption edge at 1.64 eV. Complementary transitions of the 1.55 and 1.36 eV levels occur at energies below the monochromator cutoff.

After a 150°C bakeout for 6 h, the same crystal exhibited the surface photovoltage spectrum shown in fig. 5b. The photovoltage response at all energies decreased by at least an order of magnitude.

The surface photovoltage spectrum of a clean surface obtained by cleavage at $p < 10^{-10}$ Torr is shown in fig. 5c. Two features can be seen which correspond to the absorption edge at ~1.63 eV and a transition from a bandgap level 1.42 eV below the conduction band edge. As expected, all features associated with the contaminated CdSe surface are absent. The 1.42 eV feature is not due to surface roughness since cleaved surfaces were not as smooth as initially polished faces. Identical spectra were obtained from relatively smooth and stepped portions of the same surface.

Ar^+ bombardment of the UHV-cleaved surface at 400 eV and 25 $\mu A/cm^2$ for 1 h produced a large change in the SPS features, as shown in fig. 5d. The 1.42 eV feature seems to be removed and pronounced new structure emerges which corresponds to transitions 1.05 eV below the conduction band and 1.60 eV above the valence band. The Ar^+ bombarded and cleaved spectral features were independent of previous surface treatment Ar^+ bombardment at 1 keV produced similar spectra.

The SPS features produced by Ar^+ bombardment were gradually reduced by annealing in UHV at 300°C. As shown in fig. 5e, a 4 h anneal caused only slight shifts in the Ar^+ bombarded surface energies to 1.57 and 1.18 eV, but reduced the strength of these features relative to the band gap response. For the particular spectrum shown in fig. 5e, annealing of the original Ar^+ bombarded surface reduced the excess surface Se by ~10%. This surface exhibited a sharp LEED pattern characteristic of $(11\bar{2}0)$ CdSe. Additional annealing at 300°C further reduced the peak feature so that the cpd features gradually resembled those of the cleaved surface. No additional features were produced by annealing.

Exposure of a LEED-ordered $(11\bar{2}0)$ surface to 3×10^{12} Langmuir of oxygen produced the photovoltage features shown in fig. 5f. These cpd slope changes correspond to new levels 1.61 and 0.99 eV below the conduction band and 1.66, 1.35, and 0.62 eV above the valence band. The 1.66 eV transition completely dominates any band edge absorption feature. Again, note that the transitions at 0.62 and 0.99 eV are complementary with the absorption edge. These features can not be due to bulk traps sensitized by a change in band bending since they differ significantly from the cpd features of the other surfaces. This O exposure also removes the ordered LEED pattern completely.

The SPS features produced by exposure to high oxygen pressure are similar to those produced by exposure to a 1700°C W filament at 10^{-5} Torr O_2. Fig. 6 illustrates SPS curves for various oxygen surface coverages. Surface coverages $\theta = 0.34$ and $\theta = 0.41$ were produced by the HP technique while the rest were obtained by the HF method. For all surface coverages, oxygen produces SPS features corresponding to multiple discrete levels distributed across the bandgap. The most pro-

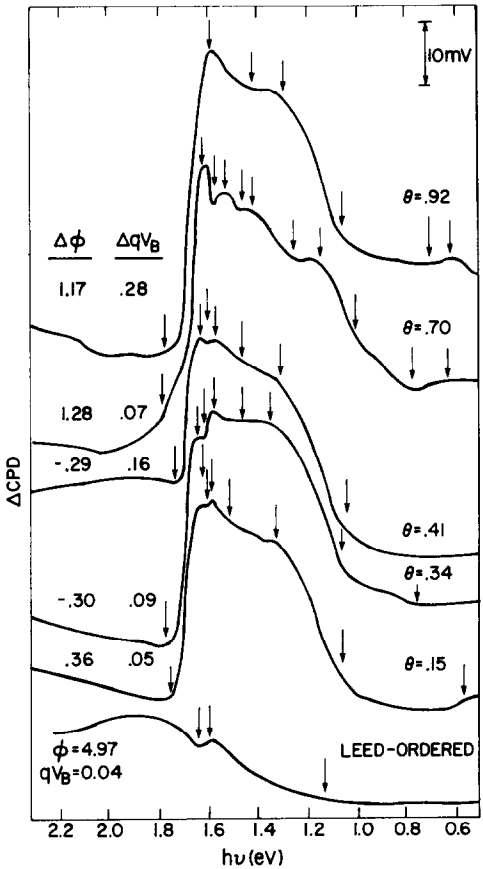

Fig. 6. Surface photovoltage spectra of clean, LEED-ordered (11$\bar{2}$0) CdSe with increasing oxygen surface coverage θ, as determined by XPS. Arrows indicate energies of maximum slope change corresponding to onsets of photovoltage transitions. The changes in surface work function $\Delta\phi_S$ and band bending ΔqV_B are given for each curve.

nounced feature corresponds to a level 1.55–1.62 eV above the valence band edge. In addition, almost all curves in fig. 6 exhibit features due to transitions involving levels 0.6 and 1.3 eV above the valence band edge and 0.7, 1.05, and 1.45 eV below the conduction band edge. Additional transition due to levels ~1.58 eV below the conduction band and 1.55 eV above the valence band were detected for $\theta = 0.15$, 0.34, and 0.41. A total of nine levels could be determined from cpd features for $\theta = 0.70$.

A relative measure of the densities of states for the O-induced, surface state levels was calculated from transient surface photovoltage measurements. A representative photovoltage transient for incident photon energy $h\nu = 1.45$ eV is illustrated in fig. 7. From the rates d(cpd)/dt measured when the monochromatic light

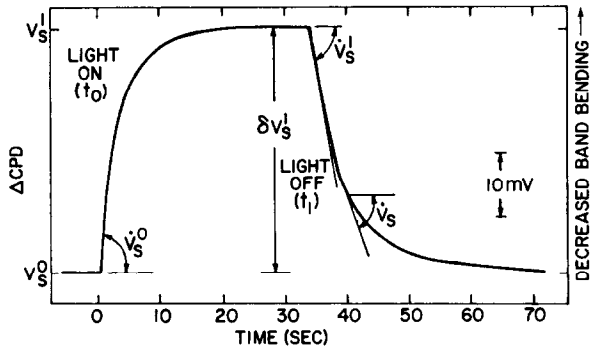

Fig. 7. Surface photovoltage transient for $\theta = 0.15$ oxygen on CdSe and illumination $I = 3.8 \times 10^{15}$ photons/cm^2 at $h\nu = 1.60$ eV; v_s^0, $\dot{v}_s^0$, v_s^1, $\dot{v}_s^1$, and $\delta v_s^1 = v_s^0 - v_s^1$ are defined at times t_0 and t_1 respectively.

is turned on ($t = t_0$) or off ($t = t_1$) and the total change in cpd, we can calculate the photoionization cross section K_{ph}, the density of electrons before illumination n_t^0, and the densities of electrons and holes after illumination n_t^1 and p_t^1 for each transition corresponding to a surface state within the band gap. For surface states in poor communication with the bulk, these parameters are obtained from [27]:

$$K_{ph} = (\dot{v}_s^0 + \dot{v}_s^1)/I\delta v_s^1 , \tag{1}$$

$$n_t^1 = -n_t^0 \frac{\dot{v}_s^1}{\dot{v}_s^0} = \frac{\alpha}{2} \frac{\delta v_s^1}{|v_s^0|^{1/2}} \frac{1}{1 + \dot{v}_s^0/\dot{v}_s^1} , \tag{2}$$

$$p_t^1 \simeq \frac{\alpha}{2|v_s^0|^{1/2}} \frac{v_s^1 - v_s}{1 - (\dot{v}_s/\dot{v}_s^1)\exp(v_s^1 - v_s)} \tag{3}$$

where $v = V/KT$ and $\dot{v}_s^0$, $\dot{v}_s^1$, v_s^0, v_s^1, and δv_s^1 are defined in fig. 7. $\alpha = (2\epsilon KT N_b/q^2)^{1/2}$, where $\epsilon = 9.7$ is the dielectric permittivity of CdSe [28], T is the absolute temperature, and $N_b = 1.5 \times 10^{16}$ cm^{-3} is the bulk electron concentration. These equations describe photostimulated depopulation of electrons from band gap states to the conduction band. By interchanging n and p and reversing voltage signs, eqs. (1)–(3) describe phototimulated population of states from the valence band as well. Contributions to the photovoltage transients from competing processes at lower energies have been effectively removed by taking differences in $\delta\dot{v}_s^1$, $\dot{v}_s^1$, and v_s^0 at energies just below and above the each transition. These energy pairs for the three major photovoltage transitions observed for $\theta = 0.15$ oxygen on CdSe are given in table 1. In each case, illumination causes a substantial change in population. Photoionization crosssections K_{ph} and total densities of states N_t are comparable to those reported for CdS [27]. Furthermore, the fractional population n_t^0 are significant only below the bulk Fermi level $E_F = 1.6$ eV above valence band,

Table 1
Surface state parameters associated with band gap levels of oxygen adsorbed on (1120) CdSe; transient photovoltage measurements of δv_s^1, $\dot{v}_s^0$, and $\dot{v}_s^1$ are defined in fig. 7; all transient voltages are normalized to illumination intensity $I = 3.8 \times 10^{15}$ photons/cm^2.

Energy range (eV)	δv_s^1 (mV)	$\dot{v}_s^0$ (mV)	$\dot{v}_s^1$ (mV)	K_{ph} (cm^{-2})	n_t^0	n_t^1	p_t^1	N_t	n_t^0/N_t
1.31–1.07	9.34	2.64	−1.40	3.5×10^{-17}	1.3×10^{10}	6.9×10^{9}	1.8×10^{10}	2.5×10^{10}	0.52
1.60–1.31	25.8	6.19	−3.61	2.6×10^{-17}	4.0×10^{10}	2.3×10^{10}	2.0×10^{10}	4.3×10^{10}	0.93
Energy range (eV)	δv_s^1 (mV)	$\dot{v}_s^0$ (mV)	$\dot{v}_s^1$ (mV)	K_{ph} (cm^{-2})	p_t^0	p_t^1	n_t^1	N_t	n_t^0/N_t
1.68–1.60	−24	−7.07	4.15	3.3×10^{-17}	3.8×10^{10}	2.2×10^{10}	1.8×10^{10}	4.0×10^{10}	0.05

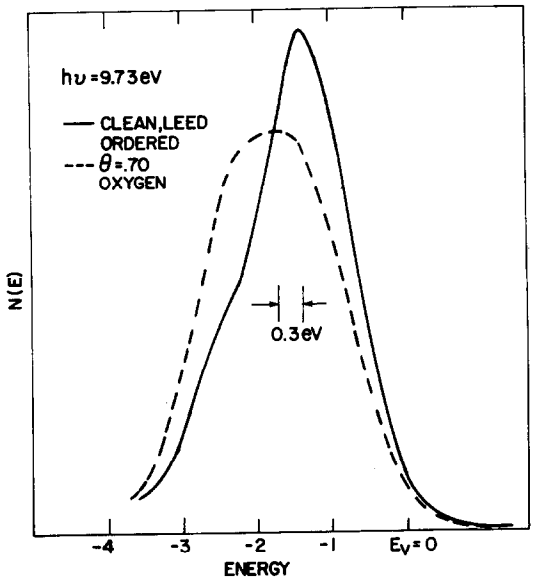

Fig. 8. Energy distributions of the photoemitted electrons for clean and $\theta = 0.70$ oxygen-adsorbed (11$\bar{2}$0) LEED-ordered CdSe; $h\nu = 9.73$ eV.

demonstrating that surface and bulk states are less isolated in CdSe than in CdS [29].

UPS and XPS measurements of O-adsorbed CdSe also show changes in electronic structure which suggest modified bonding. Fig. 8 illustrates energy distribution curves (EDC's) obtained from clean (11$\bar{2}$0) LEED-ordered CdSe before and after O adsorption. Spectra were obtained with $h\nu = 0.73$ eV at $p = 10^{-10}$ Torr (1.3×10^{-8} Pa). The EDC peak feature for $\theta = 0.70$ O on CdSe displays a 0.3 eV shift to higher binding energy, relative to the EDC of clean, LEED-ordered CdSe. A corresponding shoulder on the higher binding energy side of the valence band is observed for a $\theta = 0.98$ surface by XPS [26]. The $0.1s_{1/2}$ peak also shifts 1.1 eV to lower binding energy, as expected for oxide formation [30].

A comparison of figs. 6 and 8 illustrates the contrast in detectability of the oxygen-induced surface states by SPS versus UPS. Whereas pronounced and detailed features associated with oxygen adsorption can be measured by SPS, no photoemission from states above the valence band edge can be discerned from UPS. Furthermore UPS is not sensitive to the unoccupied surface states determined by SPS.

The extent to which bulk traps contribute to the surface photovoltage features at band gap energies has also been determined. Fig. 9 illustrates surface and bulk photoconductivity spectra for a 1.6 ohm-cm (10$\bar{1}$0) cleaved CdSe crystal in air. Only small changes in photoconductivity were observed because of the relatively low resistivity. The bulk photoconductivity spectrum shows an onset at 1.2 eV and

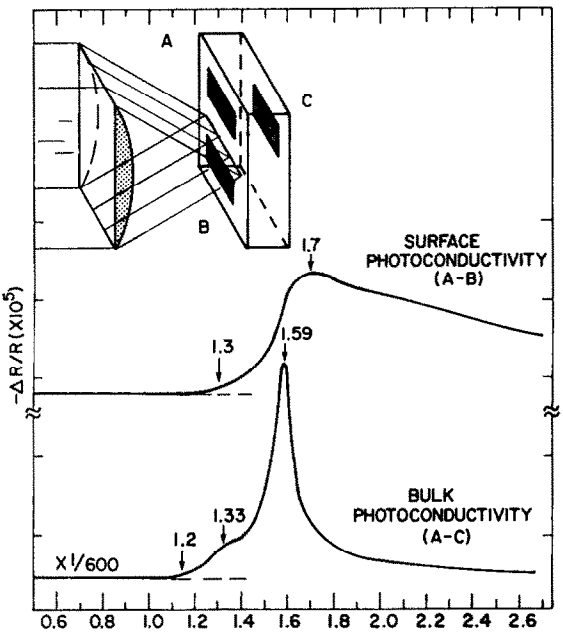

Fig. 9. Comparison of surface and bulk photoconductivity spectra for cleaved (10$\bar{1}$0) CdSe crystal in air. Distance between electrodes A and B is 0.5 mm and between A and C is 2 mm.

a distinct shoulder at 1.33 eV. The sharp decrease for $E > 1.59$ eV is due to enhanced surface absorption and recombination. The surface photoconductivity spectrum has no such feature but again shows a smooth onset at an energy 1.2–1.3 eV. Additional surface photoconductivity features could also be observed which depended on surface treatment or roughness. However, the more pronounced bulk photoconductivity structure observed below the bandgap energy for all surfaces signified the presence of at least one bulk trap level. IR absorption spectra (not shown) also exhibited a tailing from the absorption edge at 1.64 to ~1.3 eV. The photoconductivity and IR absorption spectra were the same for Eagle-Picher "ultra-high purity" (UHP), Cleveland Crystals "as-grown", and Cleveland Crystals "S-free" CdSe single crystals. None of the crystals exhibited discernible bulk inhomogeneities due to precipitated domains, as shown by an IR transmission microscope with 30 X magnification. All three types of CdSe crystal exhibited the same SPS features for (11$\bar{2}$0) CdSe cleaved in UHV, as shown in fig. 5c. SPS measurements of cleaved (10$\bar{1}$0) CdSe displayed the same spectrum.

4. Discussion

The electronic structure of (1120) CdSe surfaces as determined by SPS can now be related to the chemical structure as measured by AES, XPS, and LEED. Fig. 10

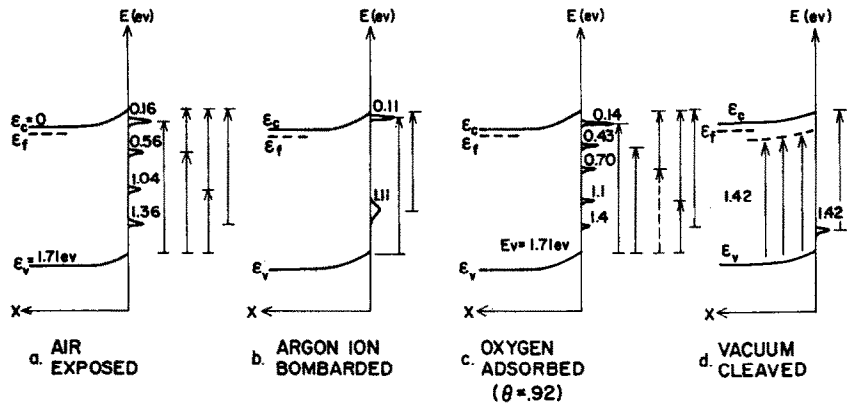

Fig. 10. Surface electronic features of (11$\bar{2}$0) CdSe under various surface conditions: (a) polished, etched, and air-exposed, (b) Ar^+ bombardment, (c) oxygen-absorbed, and (d) UHV-cleaved.

illustrates schematic energy level diagrams for the surface space charge regions of four CdSe surfaces. Fig. 10 also indicates magnitudes of surface band bending, which could be determined from the decrease in barrier height under intense UV illumination from a Xe lamp ($>10^{18}$ photons/cm^2 at $h\nu > 2.4$ eV). These magnitudes are only approximate since this illumination intensity did not produce complete photovoltage saturation (i.e. flattening of the bands at the surface).

Fig. 10a indicates the surface photovoltage transitions and associated energy levels in the band gap of polished, etched, and air-exposed (11$\bar{2}$0) CdSe. The four levels distributed across the bandgap are all associated with O, C, S, and Cl contamination. Complementary transitions into and out of two of these levels are also indicated.

Ar^+ bombardment removed these extrinsic features and introduced two new levels located 0.11 and ~1.1 eV below the conduction band edge, as shown in fig. 10b. These new states are not associated with implanted Ar^+ in CdSe [31] but rather are analogous to levels at 0.15 and 1.7 eV below the conduction band edged produced by Ar^+ bombardment of CdS [7]. As in the case of CdS, these new levels of CdSe can be related to lattice defects. Electron bombardment of CdSe at 320 keV and 77 K produces a luminescence transition at 1.1 eV and modifes the edge emission involving a level 0.1 eV below the conduction band edge [32]. Energy thresholds for these processes indicate that atomic displacement of both Cd and Se can occur. Energy levels located 0.14 and 1.1 eV below the conduction band edge have been reported for CdSe single crystals and attributed to Se vacancy donor levels and Cd vacancy acceptor levels respectively [33,34]. These results confirm our association of the Ar^+ bombardment-induced levels with the Cd–Se surface nonstoichimetry measured by AES. Furthermore, a donor level 0.14 eV below the conduction band edge agrees with out interpretation of the 1.6 eV SPS feature as that of a

photopopulating transition. The SPS features of fig. 5d are due to surface and near-surface rather than bulk lattice defects since the range of Ar^+ penetration at 400 eV is estimated to be <20 Å [31], while the penetration of band gap light is >1200 Å [35].

We can estimate a detectability limit for surface states for the Ar^+ bombarded surface from the SPS signal-to-noise ratio of fig. 5d and the relative nonstoichiometry measured by AES. The SPS features of fig. 5d are associated with a nonstoichiometry of ~10% excess Se. Since the AES sensitivity is <10 Å [23], this nonstoichiometry corresponds to $\lesssim 10^{14}$ states/cm^2 in the surface layer. A detectability limit of $\lesssim 2 \times 10^{12}$ states/cm^2 is obtained from normalization by the signal-to-noise ratio at 1.6 eV. This limit depends on the ratio $K_{ph}/K_n N_s$, where K_n is the capture cross section of surface states for electrons, N_s is the free electron density at the surface, and both are dependent on the band bending at the surface [29]. However, the surface barriers in fig. 5 do not vary substantially and other surfaces, such as $\theta = 0.15$ oxygen on CdSe exhibit a similar detectability limit. This limit is higher than the corresponding value determined for CdS [7] because of the smaller band gap and increased communication between surface and bulk [29]. Note that the detectability limit of 10^{12} states/cm^2 is greater than the densities N_t in table 1. In fact, not every lattice defect may be electrically active, thereby improving the limits of surface state detectability.

Annealing the Ar^+ bombardment surface reduces the SPS features and the nonstroichiometry initially produced by sputtering and ultimately yields a LEED-ordered surface. However, these SPS features are still detectable on the well-annealed, LEED-ordered surface, indicating that residual surface nonstoichiometry rather than any surface disorder is resposnible for these states.

The surface photovoltage transitions and corresponding energy level positions associated with oxygen adsorption on (1120) CdSe are shown in fig. 10c. The transitions are derived from the SPS features of the representative $\theta = 0.92$ spectrum in fig. 6. Again, complementary transitions are observed for all energies >0.5 eV, the cutoff energy of the monochromator. Note the ~1 eV photopopulation transition indicated by dashes which is not evident in the photovoltage spectrum because it competes with a 1.1 eV photodepopulation transition. The oxygen-adsorbed energy levels distributed across the band gap bear a strong resemblance to those of air-exposed CdSe, suggesting that oxygen is more electrically active than the other contaminants detected by AES on the "real" CdSe surface.

The SPS photopopulation feature and transient photovoltage measurements at 1.6 eV indicate an empty surface state located 1.6 eV above the valence band edge. Transitions to this state from the Cd 4d level of CdSe have also been observed from ELS measurements [25]. Field effect measurements of CdSe cleaved at 10^{-7} Torr and exposed to high O_2 pressure also reveal at least one new energy level located ~0.1 eV below the conduction band edge [36].

As noted in fig. 6, band bending qV_B increased with θ to $\theta = 0.41$, then varied irregularly. The variation in electronic structure and barrier height with increasing

coverage suggest that oxygen may adsorb by more than one mechanism. This is supported by the fact that the HP and HF methods of adsorption produce opposite changes in surface workfunction ϕ_s. As given in fig. 6, HP adsorption for $\theta = 0.34$ and 0.41 decreased ϕ_s by 0.3 eV while HF adsorption increased ϕs by 0.36–1.28 eV. Similar ϕ increases induced by the HF technique were observed for $0.25 < \theta < 0.5$ (not shown). The surface work function of LEED-ordered (11$\bar{2}$0) CdSe was determined by a combination of SPS and UPS. Furthermore the change in electron affinity $\Delta\chi$ and band bending $\Delta q V_B$ are related according to

$$\Delta\chi = \Delta\phi_s - \Delta q V_B . \tag{4}$$

Since the $\Delta\phi_s$ induced by either technique are greater than their respective $\Delta q V_B$, opposite $\Delta\chi$ changes must occur. Therefore, the two methods of oxygen adsorption produce surface dipoles of opposite sign. The increase in χ with oxygen adsorption activated by a hot filament is consistent with similar increases observed for oxygen adsorption on CdS by the same technique [14,17]. Transfer of electrons to chemisorbed oxygen [37] may well produce such an increase in χ. On the other hand, the decrease in χ with high pressure oxidation agrees with decreases in χ of cleaved CdSe exposed to a low vacuum (10^{-4} Torr or 1.3×10^{-2} Pa) [38] and may be viewed in terms of a molecular bonding which forces the negative charge at the CdSe surface back into the lattice [39]. Only surface–adsorbate interactions for $\theta < 1$ can account for these phenomena, simce multilayer adsorption ($\theta > 1$) is not observed. Campbell and Farnsworth have invoked charge exchange at low coverage ($\theta < 0.01$) and dipole formation at higher coverages to explain the adsorption kinetics and work function changes of oxygen on CdS [18]. It is noted that significant band bending changes occur for both CdSe and CdS with $\leq 10^{12}$ electrons/cm^2, equivalent to a surface coverage $\theta < 10^{-3}$ [12]. Furthermore, Somorjai has reported both donor and acceptor-type activity of oxygen on CdSe, corresponding to two mechanisms of adsorption [40].

The discrete, multiple states measured in fig. 6 can be associated with a localized molecular bonding of oxygen to the (11$\bar{2}$0) CdSe surface. These discrete states are in marked contrast to the smooth distribution of states observed for oxygen adsorbed by the same HF technique on (11$\bar{2}$0) CdS [7,14], as shown in fig. 11. This contrast can be accounted for by the difference in chemical reactivity of oxygen with CdSe versus CdS. Table 2 presents sets of possible reactions of oxygen with CdSe and CdS along with their respective heats of reaction [41,42]. The relative heats of reaction show that oxygen bonds more strongly to Cd than to Se for CdSe, where as oxygen bonding to S rather than to Cd is more favorable for CdS. This difference is significant if the initial adsorption takes place only at anion or at cation sites of the lattice. It is proposed here that initial oxygen adsorption proceeds via surface defects, in particular the anion vacancies responsible for the free electron carrier concentrations of CdSe and CdS [43]. Surface imperfections are shown to increase the chemisorptive activity of oxygen on CdS [20] and oxygen bonding to surface anion vacancies has been reported for ZnO [44]. Furthermore,

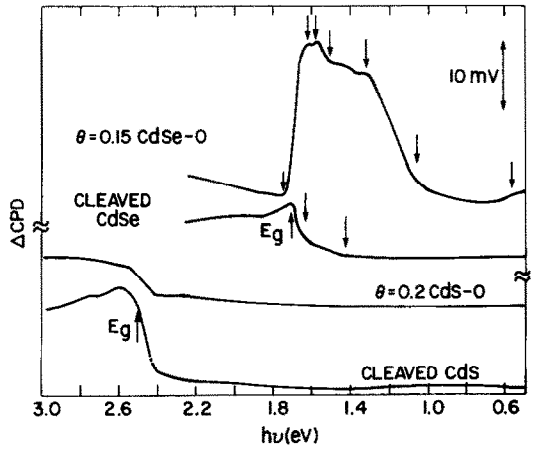

Fig. 11. Comparison between surface photovoltage spectra for oxygen adsorbed on CdSe 0.15) and CdS ($\theta \sim 0.2$). In both cases oxidation was produced by exposure to 10^{-5} Torr O_2 in the presence of a hot W filament. Band gaps E_g and discrete cpd slope changes are indicated by arrows.

the bulk carrier densities for 1 ohm-cm CdSe and CdS are $n \sim 2 \times 10^{16}$ cm^{-3} so that, assuming a uniform distribution of related bulk vacancies at the surface, oxygen bonding at each surface vacancy corresponds to $\theta \leq 10^{-4}$. This accounts for the discrete change in electrical features at very low coverages. CdSe also has ~4% larger lattice spacings than CdS [45], further increasing the relative probability that O will fill a surface vacancy. Thus O bonding to Cd atoms at these chalcogen vacancies is significantly more favorable for CdSe than CdS, thereby explaining the pronounced contrast in their SPS features.

Table 2

Heats of reaction [a] for oxygen with CdSe and CdS

Reaction	Heat of reaction (kcal/mole)
$CdSe + \frac{1}{2}O_2 \rightarrow CdO + \frac{1}{2}Se_2$	−27.9
$CdSe + O_2 \rightarrow Cd + SeO_2$	−20.6
$CdSe + O_2 \rightarrow CdO + SeO$	−13.0
$CdSe + \frac{1}{2}O_2 \rightarrow Cd + SeO$	+48.1
$CdS + O_2 \rightarrow Cd + SO_2$	−36.4
$CdS + \frac{1}{2}O_2 \rightarrow CdO + \frac{1}{2}S_2$	−26.6
$CdS + O_2 \rightarrow CdO + SO$	−25.0
$CdS + \frac{1}{2}O_2 \rightarrow Cd + SO$	+36.1

[a] Heats of formation ΔH°_{298} used for determining heats of reaction were obtained from refs. [41] and [42].

The qualitative difference in SPS features of oxygen on CdSe versus CdS can also be viewed in terms of the difference in bonding ionicity of the CdSe versus CdS surface. Mead has used bonding ionicity to interpret the difference in Schottky barrier formation of CdSe and CdS with various metals [2]. Mark has shown [46] that changes in several surface parameters of representative semiconductors exposed to oxygen scale logarithmically with the Pauling electronegativity difference of the semiconductor constituents. Application of this scaling curve to the Pauling electronegativity difference of 0.7 eV for CdSe versus 0.8 eV for CdS [47] reveals that bonding of oxygen on CdSe is >5 times active than oxygen on CdSe.

The SPS features of clean (11$\bar{2}$0) CdSe obtained by cleavage in UHV correspond to either or both of the energy level transitions shown in fig. 10d. The presence of only one feature at 1.42 eV demonstrates that all other surface electronic features of CdSe observed by SPS related to extrinsic factors such as contamination, controlled adsorption, or lattice nonstoichiometry. In contrast to SPS measurements on (11$\bar{2}$0) CdS which exhibit no intrinsic surface state or bulk traps features [7], the SPS spectra of clean (11$\bar{2}$0) CdSe show a discrete band gap level with a densiy N_t from photovoltage transients of 4.4×10^{10} states/cm^2. This is comparable to densities given in table 1 for a partially oxidized surface. The SPS spectrum shown in fig. 5c is characteristic of prismatic CdSe. Visually-smooth (11$\bar{2}$0) cleavage faces of Eagle-Picher UHP, Cleveland Crystal "as-grown" and Cleveland Crystal "S-free" single crystals all exhibit the same SPS spectrum. The 1.42 eV transition corresponds to either an intrinsic surface state or to a bulk trap level within the band gap. While cpd slope changes are observed near 1.4 eV for air-posed and O-adsorbed surfaces, no such feature appears in the Ar^+ bombarded curve. This suggests the presence of an intrinsic surface state on cleaved CdSe, since a bulk trap feature should be common to all spectra. Nevertheless, the SPS feature at 1.4 eV could be difficult to measure over the other bombardment-induced features.

On the other hand, both surface and bulk photoconductivity exhibit an onset at ~1.3 eV, indicating that a bulk trap transition takes place with approximately the same energy as observed by SPS. Such a bulk transition should exhibit cpd slope changes opposite to that of a surface transition. For example, depopulation of a surface state removes negative charge from the surface. Conversely, depopulation of a bulk level removes negative charge from the surface space change region within the photon penetration depth and thereby induces more negative charge at the surface. Thus the 1.42 eV SPS feature would correspond to population of a bulk level 1.42 eV above the valence band edge. Other measurements on vapor-phase CdSe single crystals also exhibit evidence of bulk trapping. Cathodoluminescence spectra show a dominant peak at 1.33 eV at 77 K for CdSe prior to electron beam damage [32]. Likewise, transport measurements consistently yield a donor level located at 0.3 eV [33] to 0.35 eV [36,48] below the conduction band edge with a density $0.3-1.6 \times 10^{12}$ cm^{-3} [48]. Bulk trap states have also been reported for some pure CdS crystals [6,49].

As mentioned in the Introduction, the chief significance of band gap states on

UHV-cleaved CdSe surfaces lies in their relation to Fermi level pinning at a CdSe–metal contact. The Schottky barrier heights of CdS–metal interfaces appear to scale with the semiconductor–metal work function difference, while the CdSe–metal barrier heights are relatively insensitive to this work function difference [2]. Mead accounted for this difference in term of a high density of intrinsic surface states on CdSe which "pinned" the Fermi level in a narrow energy interval within the band gap [2]. The barrier heights as measured by internal photoemission for various metals on CdSe varied only between 0.3 and 0.5 eV [50]. This behavior requires a state or set of states centered at ~0.4 eV below the conduction band edge. Clearly, an intrinsic surface state located 1.42 eV below the conduction band can not produce this Schottky barrier behavior. On the other hand, bulk traps located 1.42 eV above the valence band are at almost the exact energy position required to account for the Fermi level stabilization at the surface. Note, however, that the reported densities of such bulk trap states never exceed $\sim 2 \times 10^{12}$ states/cm^2 [48], whereas a minimum of 10^{13} states/cm^2 are required for Fermi level pinning [3,51]. On this basis, these bulk traps may or may not play a role in Schottky barrier formation. Nevertheless, the SPS measurements reported here demonstrate unambiguously that no intrinsic surface states are present on UHV-cleaved $(11\bar{2}0)$ CdSe which could account for the barrier height properties of CdSe and CdS with metals. Furthermore, other processes can influence the interface electronic characteristics. Chemical reactions are observed at interfaces of Al with CdSe and CdS which significantly alter the interface dielectric properties [52]. Likewise, unreactive metals such as Au induce extrinsic surface states in the band gap of CdS and CdSe which fall near the ultimate Fermi level position of the contact [49]. Thus both reactive and unreactive metals produce local charge redistributions at the intimate metal–semiconductor contact which can modify the Schottky barrier heights.

Conclusions

The electronic and chemical structures of CdSe surfaces have been measured by a combination of UHV techniques. With the exception of a bulk trap level common to all commercial CdSe, all electronic structure can be related to either chemical contamination or lattice nonstoichiometry. Different surface state features are measured for oxygen adsorbed on CdSe versus CdS and are related to reactivity differences at surface defects. As with CdS, no intrinsic surface states are present in the band gap of CdSe which can account for Fermi level stabilization at the metal–conductor contact.

Acknowledgements

The author wishes to thank P. Nielsen for design of the photoconductivity bridge circuit and use of his infrared miscroscope, R. Holman for use of his crystal-

cutting facilities, M. Slade for assistance with the monochromator calibration, and G. Pfister for the use of his photoconductivity equipment.

References

[1] S. Kurtin, T.C., McGill and C.A. Mead, Phys. Rev. Letters 22 (1969) 1433.
[2] C.A. Mead, Appl. Phys. Letters 6 (1965) 103.
[3] J. Bardeen, Phys. Rev. 71 (1947) 717.
[4] V. Heine, Phys. Rev. 138 (1965) A1689.
[5] C.B. Duke, J. Vacuum Sci. Technol. 6 (1969) 152.
[6] C.G. Scott and C.E. Reed, Surface Physics of Phosphors and Semiconductors (Academic Press, New York, 1975) p. 416, and references therein.
[7] L.J. Brillson, Surface Sci. 51 (1975) 45.
[8] J. Lagowski, C.L. Balestra and H.C. Gatos, Surface Sci. 29 (1972) 213.
[9] J. van Laar and A. Huijser, J. Vacuum Sci. Technol. 13 (1976) 769;
J.E. Rowe, S.B. Christman and H. Ibach, Phys. Rev. Letters 34 (1975) 874.
[10] The ellipsoidal mirror segment was produced by Special Optics, Cedar Grove, N.Y.
[11] B.D. Campbell, C.A. Hacque and H.E. Farnsworth, in: The Structure and Chemistry of Solid Surfaces, Ed. G.A. Somorjai (Wiley, New York, 1969), p. 33-1.
[12] See, for example, R. Williams, J. Phys. Chem. Solids 23 (1962) 1057.
[13] R.G. Wagner and G.C. Breitweiser, Solid State Electron. 12 (1969) 229.
[14] L.J. Brillson, J. Vacuum Sci. Technol. 12 (1975) 249.
[15] M. Yamaguchi and K. Ngai, Japan J. Appl. Phys. 13 (1974) 1897;
A.G. Sigai and H. Wiedemeier, J. Electrochem. Soc. 119 (1972) 910.
[16] M.F. Chung and H.E. Farnsworth, Surface Sci. 25 (1972) 321.
[17] B.D. Campbell and H.E. Farnsworth, Surfaci Sci. 10 (1968) 197.
[18] S.C. Chang and P. Mark, J. Vacuum Sci. Technol. 12 (1974) 624;
S.C. Chang and P. Mark, J. Vacuum Sci. Technol. 12 (1974) 629.
[19] S. Baidyaroy, W.R. Bottoms and P. Mark, Surface Sci. 29 (1972) 165.
[20] P. Pianetta, I. Lindau, C.M. Garner and W.E. Spicer, Phys. Rev. Letters 37 (1976) 1166.
[21] M.J. Katz and K.J. Haas, Surface Sci. 19 (1970) 380.
[22] L.J. Brillson and G.P. Ceasar, Surface Sci. 58 (1976) 457.
[23] J.C. Tracy, in: Electron Emission Spectroscopy, Eds. W. Dekeyser, L. Fliermans, G. Vanderkelen and J. Vennik (Reidel, Boston, 1973) p. 295.
[24] J.D.H. Donnay, Am. Cryst. Assoc. Monograph 5 (1963).
[25] L.J. Brillson, J. Vacuum Sci. Technol. 13 (1976) 325.
[26] R.H. Bube, Phys. Rev. 98 (1955) 431.
[27] J. Lagowski, C.L. Balestra and H.C. Gatos, Surface Sci. 29 (1972) 203;
C.L. Balestra, J. Lagowski and H.C. Gatos, Surface Sci., in press.
[28] D. Berlincourt, H. Jaffe and L.R. Shiozawa, Phys. Rev. 129 (1963) 1009.
[29] H.C. Gatos and J. Lagowski, J. Vacuum Sci. Technol. 10 (1973) 130.
[30] C.J. Vesely and D.W. Langer, Phys. Rev. 84 (1971) 451.
[31] C.E. Barnes, C.B. Norris, H.J. Stein and W. Beezhold, in: Ion Implantation in Semiconductors and Other Materials, Ed. B.L. Crowder (Plenum, New York, 1972) p. 333.
[32] B.A. Kulp, J. Appl. Phys. 37 (1966) 4936;
H.J. Schulz and B.A. Kulp, Phys. Rev. 159 (1967) 603.
[33] R.H. Bube, J. Phys. Chem. Solids 1 (1957) 234.
[34] R.H. Bube and L.A. Barton, J. Chem. Phys. 29 (1958) 128.
[35] M. Cardona and G. Harbeke, Phys. Rev. 137 (1965) A1467.

[36] E. Guesne, C. Sébenne and M. Balkanski, Surface Sci. 24 (1971) 18.
[37] P. Mark, J. Phys. Chem. Solids 26 (1965) 959.
[38] J.L. Shay and W.E. Spicer, Phys. Rev. 169 (1968) 650.
[39] C.B. Duke, private communication.
[40] G.A. Somorjai, J. Phys. Chem. Solids 24 (1963) 175.
[41] K.C. Mills, Thermodynamic Data for Inorganic Sulphides, Selenides, and Tellurides (Butterworths, London, 1974).
[42] O. Kubaschewski, E.LL. Evans and C.B. Alcock, Metallurgical Thermochemistry, 4th ed. (Pergamon, Oxford, 1967) pp. 303 ff.
[43] F.A. Kröger, H.J. Vink and I. van den Boomgard, Z. Physik. Chem. 203 (1954) 1.
[44] W. Göpel, Surface Sci. 62 (1977) 165.
[45] W.R. Cook Jr., J. Am. Ceram. Soc. 51 (1968) 518.
[46] P. Mark and W.F. Creighton, Appl. Phys. Letters 27 (1975) 400.
[47] L. Pauling, The Nature of the Chemical Bond, 3rd ed. (Cornell Univ. Press, Ithaca, 1960) p. 93.
[48] C. Manfredotti, A. Rizzo, L. Vasanelli, S. Galassini and L. Ruggiero, J. Appl. Phys. 44 (1973) 5463, and references therein.
[49] L.J. Brillson, in: Proc. 13th Intern. Conf. on Physics of Semiconductors, Ed. F.G. Fumi (Typografica Marves, Rome, 1976), p. 665.
[50] C.A. Mead, Solid State Electron. 9 (1966) 1023.
[51] D.V. Geppert, A.M. Cowley and B.V. Dore, J. Appl. Phys. 37 (1966) 2458.
[52] L.J. Brillson, Phys. Rev. Letters 38 (1977) 245.